Seismic reliability of base isolated systems: sensitivity to design choices

SEISMIC RELIABILITY OF BASE ISOLATED SYSTEMS: SENSITIVITY TO DESIGN CHOICES

F. Micozzi [(1)], F. Scozzese *[(1)], L. Ragni [(2)], A. Dall'Asta [(1)]

[(1)] University of Camerino, {fabio.micozzi; fabrizio.scozzese; andrea.dallasta}@unicam.it

[(2)] Polytechnic University of Marche, laura.ragni@staff.univpm.it

Abstract. Seismic isolation is considered an effective solution to protect buildings and related content from earthquakes, and consequently reduce seismic losses. However, the overall reliability levels achieved on these systems by following the design rules suggested by codes are not uniform and they may be strongly influenced by some choices made in the structural design. This study aims to investigate the seismic reliability of structural systems equipped with high-damping rubber bearings, which is a widely used class of isolators. An extensive parametric analysis is performed to assess the influence of design choices on the failure probability, considering design parameters concerning both the isolation system and the superstructure, such as: isolation period; bearings shear strain; percentage of flat sliders (i.e., bearing shape factors); superstructure overstrength ratio. A set of case studies have been configurated by varying and combining all the aforesaid parameters. A stochastic model is used for the bidirectional seismic input and the generation of horizontal ground motion components, whereas full probabilistic analyses are performed via Subset Simulation to achieve accurate estimates of the demand hazard curves up to very small failure probabilities. To reduce the computational effort, a 3D-model with a reduced number of DOFs (Degrees of Freedoms) is adopted for each case study. It consists of an uncoupled bidirectional elastoplastic model of the superstructure, and an advanced nonlinear 3D model of the rubber isolators, accounting for the coupling between vertical and horizontal response in large displacements. For each case analysed, demand hazard curves are evaluated to illustrate the probabilistic properties of the seismic response for both isolation system and superstructure. Results show a noticeable sensitivity of the system reliability with respect to the examined design choices and in some cases the achieved structural performance can be far from the safety levels required by the Codes.

Keywords: seismic isolation design, rubber bearings, seismic reliability, Subset Simulation, stochastic model, overstrength factors.

1 Introduction

This paper focuses on seismic base isolation with High Damping Rubber (*HDR*) bearings, which is an efficient and widely used technique for passive seismic protection of buildings and related content [1][2]. In general, seismic isolation drastically reduces the structural and non-structural damage even in the case of earthquakes of medium-high intensities, notably shortening the post-event recovery time and enhancing structures resilience. Most of the modern codes adopted by earthquake prone countries include prescriptions about the design of isolated structures; however, systems designed in accordance with these standards, based on deterministic and conventional design value of the seismic intensity, can show very different performances under extreme events. Consequently, the reliability, measured in terms of the mean annual frequency (*MAF*) of failure, can result significantly inhomogeneous case by case.

Isolated buildings can be seen as in-series systems in which two main structural components are involved: the isolation system and the superstructure. Both these components may exhibit anticipated failure potentially lowering the overall robustness of the system (i.e., the failure of a single component can lead to the collapse of the whole structure). Moreover, even if the isolation system does not fail, the stiffening behaviour at large displacements of *HDR* bearings may cause an increase of the base shear leading to a brittle collapse of the superstructure, as it is not designed for a large ductile behaviour.

Recent studies [3] highlighted that current code prescriptions for isolator production or qualifications may be sometimes inadequate to guarantee that bearings are able to face events significantly larger than the design one. Thus, the calibration of adequate safety factors is essential to achieving satisfactory safety levels. For example, the actual displacement capacity of *HDR* bearings under horizontal and vertical loads is a key parameter controlling the failure, but the current version of EN15129 [4] (i.e., the European standard for seismic isolation devices) prescribes a strength test (called "lateral capacity test") up to a shear deformation only a little greater than the reference value used in the design. Consequently, in the European context the collapse deformation is not actually known by the manufacturer neither by the structural designer. The American seismic code [5] also presents similar limits, as recently highlighted in [3] and demonstrated in detail by Kitayama and Constantinou [6] and Shao et al. [7] for friction isolators. Furthermore, prescriptions for superstructure strength are not consolidated and are still matter of discussion [6][7][8][9][10]. Therefore, while code conforming traditional solutions are characterized by adequate reliability levels (procedures to make high quality structural components are consolidated as well as safety coefficients to be used in the design), code conforming base-isolated structures may show reliability levels below the target suggested by the design codes [11][12]. At this regard, American code [5] prescriptions for seismic design requires an "absolute" collapse probability lower than 1% in 50 years, and this limit value is going to be implemented in the future revisions of Eurocodes too, as illustrated in [11].

In order to assess whether the probability of structural collapse is under the target reliability level, seismic reliability analyses must be carried out by using proper probabilistic approaches, as recently carried out for structures equipped with dissipation devices which suffer similar issues [13][14][15][16][17], and for base-isolated structures equipped with different kinds of isolators [6][18][19].

However, most of the previous studies and relevant conclusions about the system reliability are based on simplified mechanical behaviours of *HDR* bearings (e.g., equivalent elastic or elastoplastic) [1][19] and/or deduced from a planar seismic analysis (neglecting the effects related to the two-directional behaviour of isolators and structures [6][7][18][20]). Recently, some code-conforming case studies have been analysed [21][22][23][24] by considering a bi-directional input [25] and advanced 3D nonlinear models for *HDR* bearings and unsatisfactory failure rates have been observed in these studies too. Nevertheless, a deeper analysis is required to consolidate these observations, especially because most of the previous studies are focused on specific single case studies instead of looking at a wide range of possible case studies resulting from the design process.

For this reason, in this paper, a systematic study on the role of design parameters choice on the overall reliability is investigated to evaluate the potential variation of the failure probability respect to required target values. In particular, the following parameters have been considered and varied within the range of most common values: isolation periods; bearings design shear deformation; percentage of flat sliders (i.e., the number of *HDR* bearings and flat sliders, if any, respect to the overall number of bearings); design overstrength ratio (i.e., the ratio between the actual superstructure base shear strength and the superstructure base shear demand at the design condition). A set of case studies are configured by varying and combining all the aforesaid parameters.

Probabilistic analyses are performed via Subset Simulation [26][27], which is an efficient and robust tool able to provide accurate estimates of the demand hazard curves up to very small failure probabilities, which is essential especially in the case of strategic structures in which the reliability level must be higher than standard structure [28][29][30]. A stochastic model is used for the bidirectional seismic input characterization, whose parameters have been calibrated to be representative of Italian high seismicity zones. Moreover, to reduce the computational effort of analyses, a 3D-model with a reduced number of DOFs is adopted for each case study. It consists of an uncoupled bidirectional elastoplastic model of the superstructure, and an advanced 3D nonlinear model of the *HDR* bearings , accounting for the coupling between vertical and horizontal response in large displacements [31][32][33]. The choice of this simplified 3D-model allows considering the characteristic bidirectional behaviour of isolation system keeping as low as possible the computational effort [13] and enabling the use of a full probabilistic approach.

The influence of the above parameters on the seismic response of the system is evaluated by providing a comparison in terms of demand hazard curves for the two main demand parameters: the maximum relative displacement of the superstructure and the maximum shear deformation of the isolation system. Results are discussed and useful insights are provided about the safety margins needed to obtain adequate reliability levels of base-isolated systems. In details, the paper is structured as follows: first the probabilistic framework is introduced, by presenting both the reliability analysis tool and the stochastic hazard model; then the case studies and their design are presented, along with the relevant modelling strategy; finally, the outcomes of the parametric investigation are discussed, and conclusions are provided.

2 Probabilistic method

This section describes the probabilistic framework used to perform seismic reliability analyses on base-isolated systems. The framework consists of an efficient probabilistic tool, Subset Simulation [26], and a stochastic ground motion model for seismic hazard characterization and bidirectional seismic samples generation.

2.1 Reliability analysis

Seismic reliability analysis aims to assess the probability of a structural system attaining an unsatisfactory performance at least once within a reference time frame. The system response subjected to the seismic hazard is described by the random variable *D*, whose recurrence properties over time are expressed by the mean annual frequency (*MAF*) of exceedance of a threshold *d*:

$$\nu_D(d) = \bar{\nu} G_D(d) \tag{1}$$

with $\bar{\nu}$ denoting the *MAF* of occurrence of at least one event within the range of intensities of interest, which is a function of the seismic scenario (location of seismic source and recurrence properties of seismic events), and $G_D(d) = P[D > d]$ characterizing the probability of exceedance of a threshold d of the demand parameter *D*, given the occurrence of any earthquake of intensity higher than the minimum expected from the source (i.e., consistent with $\bar{\nu}$). To perform a reliability analysis, the function $\nu_D(d)$ must be estimated over a wide range of threshold values to characterise the probabilistic response of the system from the highest up to the lowest probabilities of exceedance. Being the *MAF* $\nu_{target} = 2 \cdot 10^{-4}$ 1/year the target reliability level commonly required by the Codes for structural systems [11][12], the systems' reliability and failure conditions should be assessed at least up to this *MAF* value.

To achieve this aim, different probabilistic approaches could be used, such as (direct) simulation-based methods or conditional approaches. The first class of methods consists of tools based on the observation of the system response to samples drawn from the probability distribution of the random inputs (e.g., earthquake characteristics, structural model) and encompasses methods like Monte Carlo simulation [34] and the more efficient variance reduction techniques, such as Importance Sampling [35] and Subset Simulation [26]. The methods belonging to the second class have been developed in the last 20 years, since the seminal works of Cornell et al. [36], with the main purpose of making seismic reliability and risk estimation more practice-oriented and computationally affordable. The latter methods are widely adopted within the performance-based earthquake engineering (PBEE) approach [37] proposed by the Pacific Earthquake Engineering Research Center (PEER) [38][39].

In this study, the robust Subset Simulation [26] is used for estimating accurate demand hazard curves within the range of *MAFs* from 10^{-1} to 10^{-5} 1/year. The basic idea behind this advanced simulation technique is to express the rare-event probability $G_D(d_l)$ in terms of the product of larger conditional probabilities, by introducing intermediate exceedance events corresponding to lower threshold values $d_1 < d_2 < \ldots < d_l$. In the analyses, the original implementation [27][40] of the method is employed. This relies on the Markov Chain Monte Carlo algorithm and the Metropolis–Hastings sampler to generate samples conditional on the intermediate failure regions and thus gradually populate from the frequent to rare event region in an efficient way. Assuming a fixed value p_0 for the conditional probabilities of exceedance of the various thresholds, each time a set of n_{sim} samples is generated through the Metropolis-Hastings algorithm (standard Monte Carlo simulation for the first threshold), and the corresponding demand threshold d_i is simply evaluated as the $(1\text{-}p_0)n_{sim}$-th largest value. The exceedance probability of the i-th threshold, computed by carrying out i-times the product of the same probability p_0, is p_0^i, for i=1, 2, ..., l, and the lowest obtained value of the failure probability is p_0^l.

In this study, demand hazard curves are estimated by performing, for every case of analysis, a set of 10 independent runs of Subset Simulation and by taking their average. In this way, the obtained results have a level of accuracy comparable to that of a robust direct Monte Carlo analysis performed with millions of simulations [27][40].

2.2 Stochastic ground motion model

A direct simulation approach such as Subset Simulation requires a reliable stochastic representation of the bidirectional seismic input to achieve an accurate estimate of small failure probability. In this paper, the flexible and widely used stochastic point source simulation method of Boore [41] is employed in conjunction with the Atkinson-Silva [42] source-based ground motion model. These allow generating ground motion samples conditional to the features of a given seismic scenario, specified by two main random variables, the moment magnitude M, and the epicentral distance R. The moment magnitude is assumed to follow the Gutenberg-Richter recurrence law [43][44], $\nu_M(m) = 10^{(a-bm)}$, with parameters a and b characterising the seismic source (mean number of earthquakes expected) and the regional seismicity (factor governing the proportion of small to large earthquakes), respectively. Given an earthquake event, the aforesaid recurrence law bounded within the range of magnitudes of interest [m_0, m_{max}] leads to the following probability density function of M (with $\beta = b \cdot log_e(10)$).

$$f_M(m) = \beta \frac{e^{-\beta(m-m_0)}}{1 - e^{-\beta(m_{max}-m_0)}} \tag{2}$$

The probability density function of R is obtained under the hypothesis that the source produces random earthquakes with equal likelihood anywhere within a distance from the site r_{max}, beyond which the seismic effects are assumed to become negligible.

The procedure for the simulation of two horizontal ground motion components is summarised below and follows from [41][42] as modified by [45]. A pair of seismic acceleration time series is obtained by modulating in time two white noise signals, $w_i(t)$ (with t denoting time and i = 1, 2), by means of the shape function $e(t)$; the Fourier transform $\bar{Z}_i(\omega)$ of the resulting time-functions $z_i(t) = e(t)w_i(t)$ (normalized to have unitary mean square amplitude) are then multiplied by the target radiation spectra $S_i(\omega) = \varepsilon_i A(\omega)$, where $A(\omega)$ is a deterministic function of the angular frequency ω while ε_i are random scaling factors accounting for the spectral amplitude variability; the desired ground motion acceleration time series $a_i(t)$ can be finally obtained by the inverse Fourier transform of the function $\varepsilon_i A(\omega)\bar{Z}_i(\omega)$. It is worth noting that both the time modulating function and the radiation spectrum depend (also) on seismic scenario and site-related parameters (i.e., the moment magnitude, the epicentral distance and the local soil conditions) although (for simplicity of notation) such dependency was not made explicit in the description provided above. For sake of clarity, Fig. 1 illustrates the variability with the magnitude (at fixed epicentral distance 20 km) of both the radiation spectra and the time-envelope functions.

The two scaling parameters, ε_1 and ε_2 (also called random scaling disturbance), are modelled as lognormal random variable having unit median, standard deviation $\sigma_{ln\varepsilon} = 0.523$ (similarly to what suggested by [40] for unidirectional seismic actions) and correlation $\rho = 0.8$ [46]. The random scaling disturbance (ε_1, ε_2), together with the Gaussian white noise process, ensure that the ground motions record-to-record variability is accounted for, in terms of energy content variability within both the time and frequency domain. The resulting overall variability provided by the model is shown through the plots of Fig. 2a and Fig. 2b, which depict the response spectra of pairs of horizontal components for different values of magnitudes and the corresponding acceleration time series, respectively.

To summarise this section, the random properties of the seismic ground motions are described by the set of variables $\{M, R, \varepsilon, \boldsymbol{W}\}$, being $\boldsymbol{W}$ the $2 \times K$ matrix collecting the stochastic white-noise processes $w_1(t)$ and $w_2(t)$, each of which is modelled through an independent K-dimensional Standard

Gaussian vector $\boldsymbol{W}_i$ ($i = 1, 2$) with elements $w_{i,k}$ ($k = 1, 2, \ldots, K$) evaluated at discrete time instants $t_k = k\Delta t$, consistently with the finite time interval Δt adopted to perform the numerical integration. The rest of the scenario's parameters (e.g., *a* and *b* related to the Gutenberg-Richter law, the shear-wave velocity V_S30 characterising the seismic response amplification of the soil, etc.) are fixed parameters.

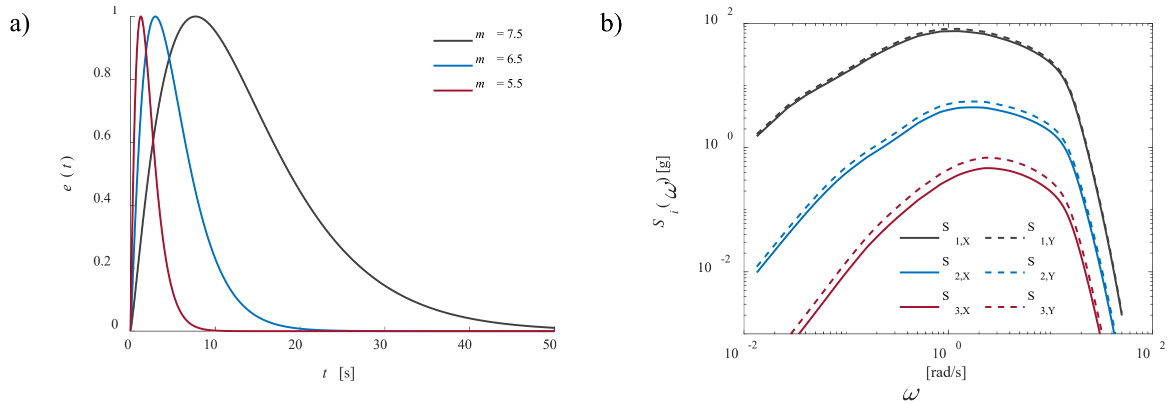

Fig. 1. Time-envelope functions (a) and Target Fourier spectra (b) of pairs of horizontal components for r = 20 km and different M values.

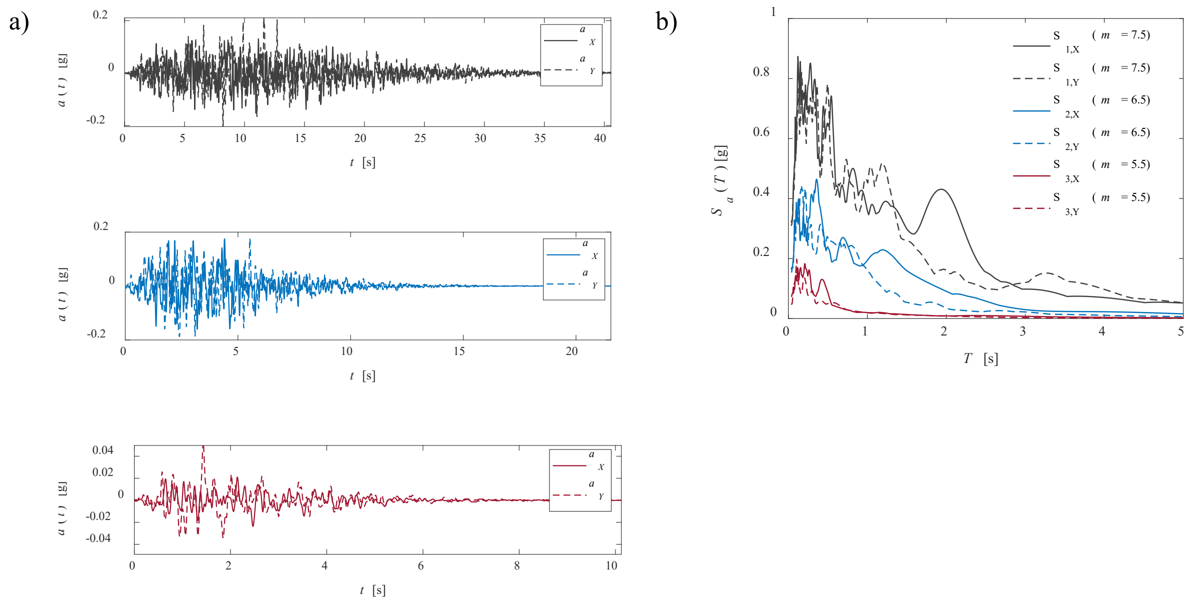

Fig. 2. Acceleration time series (a) and Response spectra (b)for three pairs of horizontal seismic components corresponding to different magnitudes (at r = 20 km).

2.3 Seismic hazard

A seismic hazard representative of Italian high seismicity zones is adopted in this study. The following set of parameters governing the stochastic hazard model is selected, also according to the existing literature [43][47][48]: $m_0 = 5.5$, $m_{max} = 8$, $a = 4.35$ and b=0.9, $r_{max} = 50$ km. A shear wave velocity V_{S30} equal to 255 m/s has been chosen as representative of deformable soil conditions at the site [49].

Although a direct simulation approach is used in this study to perform seismic reliability analyses, an Intensity Measure (*IM*) has been introduced to carry out the design of all the considered case studies: according to the current concept of partial safety factors, the *IM* is used to quantify the seismic intensity at the design rate of occurrence prescribed by the codes. Many different *IM* can be chosen, but an efficiency evaluation specifically made for isolation systems [50] suggests that the best choice is the $S_{aRotD100}(T,\xi)$ [50][51], combined with the recently proposed strategy of averaging the spectral values over a period range ([52][53]), rather than computing them at a given single T value. The resulting *IM*, denoted as $AvgS_{aRotD100}$, is expressed as follows:

$$AvgS_{aRotD100} = exp\left\{\frac{1}{N_T}\sum_{i=1}^{N_T} ln[S_{aRotD100}(T_i)]\right\} \tag{3}$$

being N_T the number of periods in which the considered range $[T_{1,}T_{N_T}]$ is discretised; the inherent damping rate ξ, implicit in the above expression, is assumed equal to 5.0%. It is worth noting that the use of an average *IM* over a range of periods better allows to cope with the variability of the *HDR* bearings dynamic response with the strain amplitude and repeated cycles [54].

The isolation systems analysed in the following are characterized by two different isolation periods, T_{is}=3.0 s and T_{is}=5.0 s, hence two IM_s (IM_{3s}, IM_{5s}) with two different ranges of periods have been adopted: from 2.0 s to 4.0 s for the T_{is}=3.0s isolation system, from 4.0 s to 6.0 s for the T_{is}=5.0s one. Both the intervals have been discretized by steps of 0.1 s.

The *IM* hazard curves obtained for the scenario defined above via Subset Simulation (according to the method of [55]) are depicted in Fig. 3, along with some further information provided to ease the understanding of the design strategy discussed later. The curves averaged on 10 independent runs ([27][40]) are assumed as *IM* curves (red solid lines identify the average, grey lighter curves the single runs); the horizontal black dotted line identifies the design hazard level considered by the European codes [56], represented by a *MAF* of exceedance ν_d = 0.0021 1/year (probability of exceedance of 10% in 50 years), which corresponds to the intensities im_d = 0.173 *g* for the T_{is}=3.0s isolation system and im_d = 0.071 *g* for the T_{is} =5.0s one (*g* is the gravity acceleration), as highlighted by the yellow dots in the chart. Finally, the blue circle markers added to the plot show both intensities and *MAF*s of the ground motion samples used to design the isolation systems (each circle corresponds to a pair of ground motion components, being the chosen *IM* direction-independent). As better described in Section 3.3, 100 accelerograms are generated to design the base-isolated systems, so that to have *IM*s as close as possible to the target *IM* values (im_d).

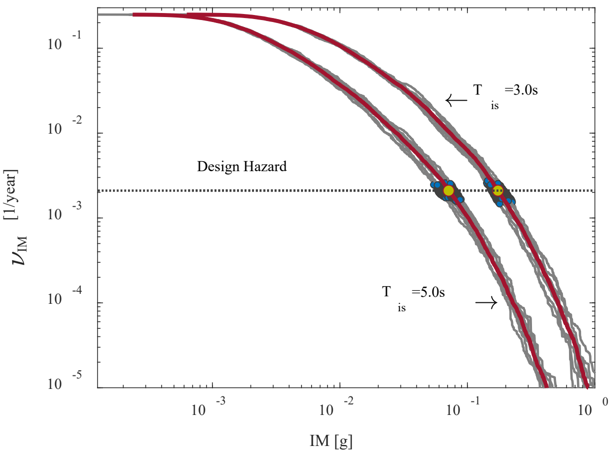

Fig. 3. IM hazard curves and design conditions for two isolation periods: 3.0s, 5.0s.

3 Parametric analysis

3.1 Case studies and parameters investigated

The design process of isolated structures involves a series of design choices. To assess their effect on the structural reliability, an extensive parametric analysis has been performed considering one archetype building and by varying the following set of design parameters: isolation periods T_{is}; bearings design shear deformation γ_d; percentage of flat sliders; design overstrength ratio (i.e., the ratio between the superstructure base shear capacity and the superstructure base shear demand at the design condition). More in detail, the following archetype building is selected as case study (Fig. 4): a four-storey reinforced concrete (r.c.) building (total height 12m) with 1 kNs^2/m^3 distributed mass for each floor (5 floors including the base floor above the isolation system), 2 x 4 spans of 5m each, and 15 columns, for a total mass of 1000 kNs^2/m.

For what concerns the variable design parameters, two isolation periods, equal to T_{is}=3s and T_{is}=5s, have been considered: the former is somehow a current common value for new isolated buildings whereas the latter is an upper limit value for residential buildings. Regarding the design shear deformation, three values are considered, i.e., γ_d =1, γ_d =1.5 and γ_d =2, which are all lower than the limit of 2.5 imposed by the European code on anti-seismic devices [4] and around common values (1.5) currently used by designer in European countries.

Two different device configurations have been investigated by varying the number of rubber bearings (N_{is}): with only rubber bearings (a total of 15 *HDR* bearings, one under each column) and with a combination of rubber bearings and flat sliders (8 *HDRs* and 7 flat sliders, placed according to the configuration of Fig. 4a).

Another design parameter considered in the parametric study is the superstructure strength, which depends on the seismic demand at the design condition as well as on the design prescriptions and safety factors. At this regard, for isolated structures, the Eurocode [56] allows designing with a reduced value of the seismic lateral force by adopting a behaviour factor q falling in the range [1, 1.5]; similarly, ASCE 7 [5] prescribes q values in the range [1.0, 2.0]. These Codes' indications are based on the hypothesis that the minimum superstructure yielding strength is higher than the design value magnified by q, due to safety factors applied to material strengths and a minimum structure redundancy [57]. The ratio between the design base shear and the actual yielding force of the system is generally defined over-strength factor, Ω, which may be notably higher than the behaviour factor q, especially for isolated structures (up to a value of 2.5 [22]), because of other superstructure strength sources stemming from non-structural elements (e.g., strong infill panels) and non-seismic actions (gravity and wind loads). It is therefore useful to define an overstrength ratio Ω/q which directly expresses the ratio between the actual strength capacity and the seismic demand. Considering the limit values for both q and Ω, the two limit cases of Ω/q=1.0 and Ω/q=2.5 have been analysed in this work, according to q-Ω pairs equal to 1.5-1.5 and 1.0-2.5 respectively.

Given the already high number of variable parameters (as detailed above), the fixed-base fundamental period of the superstructure is set as constant parameter, equal to T_s = 0.5s regardless of the overstrength ratio Ω/q.

A total of 12 case studies have been configured by varying and combining all the aforesaid parameters, as summarised in Table 1.

The last case study (case 12) has the specificity of having the same superstructure yielding strength of the case 4 (T_{is}=3s and Ω/q=2.5) and an isolation system designed with T_{is}=5s. The resulting value Ω/q is equal to 4.75 due to the lower design base shear of T_{is}=5s. Indeed, this case has been considered with the aim of showing how a higher isolation period can improve the structural seismic performances without graving too much on the costs of the superstructure.

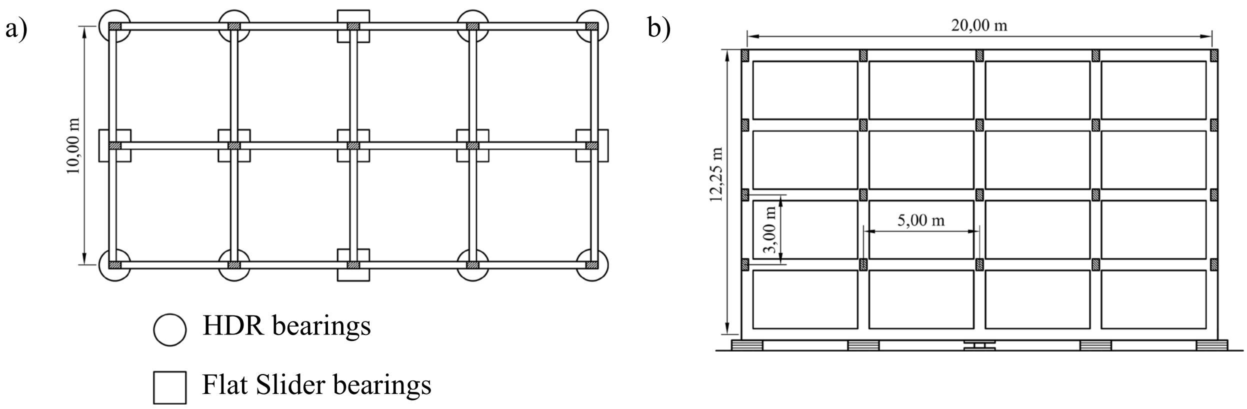

Fig. 4. Plan view of the second bearing configuration (a) and section views of the case study (b) (configuration with 8 rubber bearings and 7 flat slider)

Table 1. Case studies considered in parametric analysis.

Case	T_{is} [s]	γ_d [-]	N_{is} [-]	Ω/q [-]
1	3.0	2.0	15	1.0
2	3.0	1.5	15	1.0
3	3.0	1.0	15	1.0
4	3.0	2.0	15	2.5
5	3.0	1.5	15	2.5
6	3.0	1.0	15	2.5
7	3.0	2.0	8	1.0
8	3.0	1.5	8	1.0
9	3.0	1.0	8	1.0
10	5.0	2.0	8	1.0
11	5.0	2.0	8	2.5
12	5.0	2.0	8	4.75

3.2 Numerical model

A numerical model is developed for each case study with the aim of reducing as much as possible the computational cost of probabilistic analyses (i.e., high number of simulations, each requiring the solution of a nonlinear-time history analysis of the base-isolated structure), without losing the accuracy in terms of the complex *HDR* bearing behaviour. Indeed, differently from past studies, where simplified mechanical behaviours of *HDR* bearings (e.g., equivalent elastic or elastoplastic) [1][18] and/or planar models were considered ([6][7][18][20]), the present work exploits a refined modelling approach, which takes origin from the two-degree of freedom (2-DOF) model proposed by Kelly [1][58]. According to [1], the dynamic response of a multi-degree of freedom model (M-DOF) can be efficiently assessed using an equivalent 2-mass model (Fig. 5), able to account for both the isolation and the first fixed base modal contributions to the dynamic response. In the current study, this concept has been extended to a bidirectional seismic input (6 degrees of freedom), considering the complex nonlinear behaviour of the rubber.

More in detail, the model consists of two masses, m_b and m_s, both related (but not equal) to the mass of the base slab and the deformable super-structure. To guarantee the dynamic equivalence of the response between the two mass model and a full M-DOF model, the two masses m_b and m_s should be chosen in such a way that m_s is equal to the effective mass of the first fixed base superstructure mode while $m_s + m_b$ is equal to the total mass of the building M (including the base slab mass). Given the features of the building, the ratio between the effective mass of the first fixed base superstructure mode and the total mass of the system has been assumed equal to 0.6 [1], i.e., $m_s = 0.6M$ and $m_b = 0.4M$.

The motion of m_b with respect to the ground is described by the vector $\mathbf{u}_b = \left[u_{bx}, u_{by}, u_{bz} \right]$ collecting the motion component along two horizontal directions and the vertical direction. The motion of the mass m_s relative to m_b is described by the vector $\mathbf{u}_s = \left[u_{sx}, u_{sy} \right]$, neglecting the vertical relative motion of the two masses. The dynamic balance equations can thus be formulated as follows:

$$
\begin{aligned}
-\mathbf{f}_s(\mathbf{u}_s) &= m_s(\ddot{\mathbf{u}}_s + \ddot{\mathbf{u}}_b + \ddot{\mathbf{u}}_g) \\
\mathbf{f}_s(\mathbf{u}_s) - \mathbf{f}_b(\mathbf{u}_b) &= m_b(\ddot{\mathbf{u}}_b + \ddot{\mathbf{u}}_g)
\end{aligned}
\tag{4}
$$

where $\mathbf{u}_g$ is the ground motion and $\mathbf{f}_s$, $\mathbf{f}_b$ describe the response forces due to the super-structure and the isolation system. As for the displacement vectors, $\mathbf{f}_b = [f_{bx}, f_{by}, f_{bz}]$ is a three component vector deriving from the Kikuchi bearing element [32] used in the model while $\mathbf{f}_s = [f_{sx}, f_{sy}]$ is the two component force representing the superstructure base reaction.

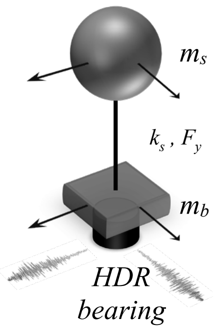

Fig. 5. Scheme of the equivalent 2-mass model adopted for the isolated structures

Regarding the mechanical behaviour of the isolation bearings, the Kikuchi bearing element [32] available in the Opensees software [59] has been used. It is a fully coupled three-dimensional model able to capture the buckling and post-buckling behaviour (i.e. the interaction between the coupled bi-dimensional horizontal behaviour and the axial force). More in detail, the model is composed by two sets of axial springs (one at the top and the other at the bottom of the element) and a radial distribution of shear springs at the mid-height of the element [31]. The large displacement formulation permits to reproduce nonlinear geometric effects, i.e. the horizontal and vertical stiffness reduction due to the rise of vertical loads and horizontal displacements, as originally proposed by Kelly [1][58]. This capability appears very important especially for medium-high level of vertical pressure and high displacements, where the buckling load could be attained (usually assumed as the condition with zero tangent stiffness of the horizontal response) and the post-buckling behaviour could take place up to the theoretical loss of vertical load capacity. This is also influenced by the hardening behaviour at large shear strains, which strongly depends on the rubber compound used for the bearings. In particular, the Kikuchi bearing element requires a model for the nonlinear behaviour of the shear springs, and in this study the *KikuchiAikenHDR* material has been used (code X0.40MPa). The nominal equivalent elastic parameters (i.e., the shear modulus G_{eq} and the damping ratio ξ_{eq}) [4] of high damping rubber bearings belong to the Bridgestone rubber compound X0.4S [60] and are illustrated in Fig. 6b and Fig. 6c (black dotted line) as a function of the shear strain γ. The other curves represent the equivalent elastic parameters coming from the numerical cycles reported in Fig. 6a, with reference to a bearing used in the design, as better specified later. It is worth to note that in the considered case, the reduction of stiffness due to the increment of vertical load is evident although the hardening behaviour at large strain is prevalent with respect to the softening behaviour due to the vertical stress.

The Kikuchi Bearing Element is also a geometry-influenced model, i.e., describes the response of a single bearing and it explicitly depends on the real diameter and height of the isolator.

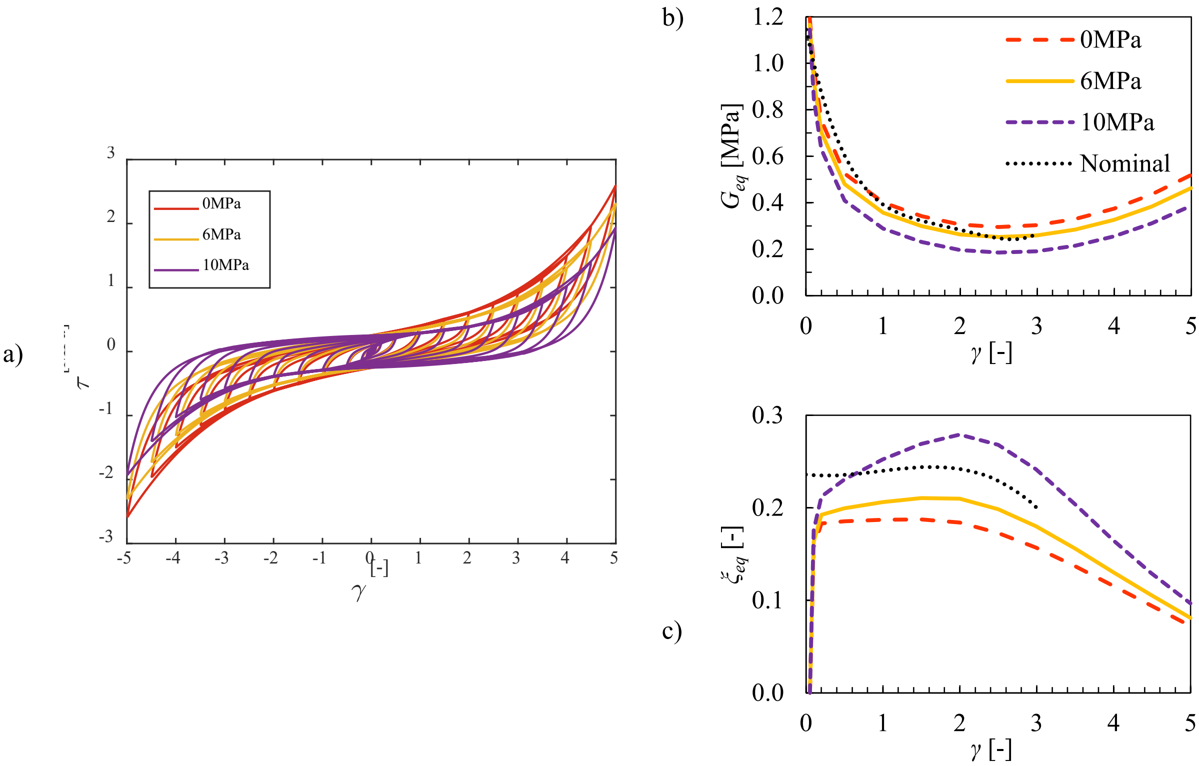

Fig. 6. Behaviour of the *HDR* bearing with 427/158/3 D_{is}=427mm, h_{is}=158mm at different pressures (a); Nominal and numerical equivalent linear parameters of the rubber X0.4S [60] (b, c).

To describe the response of the whole base-isolation system by a single element, as assumed in this study, it is necessary to introduce the following assumptions: 1) the rubber bearings have all the same geometry, 2) they support almost the same amount of vertical load (computed during the design process) and 3) the base slab of the structure is stiff enough to be well approximated by a diaphragm constraint. With these assumptions the model provides a satisfactory approximation of the real behaviour of base-isolated building, except for the overturning effect leading to a variable axial load during the seismic event. However, this effect is negligible for low-rise buildings [61] as the archetype building considered in this paper. Regarding flat sliders, under the assumption of negligible friction coefficients and very high displacement capacity, their contribution is neglected within and for the purposes of the present study, although slight response modifications might arise from their explicit consideration in the model [20][22][23].

As already mentioned, the superstructure has been modelled by two uncoupled elastoplastic springs with stiffness k_s and yielding force F_y, describing the behaviour of the superstructure frame along the two main horizontal directions. The choice of uncoupled springs instead of a coupled (isotropic) behaviour for the elastoplastic response is driven by the observation that frames and infill panels, which provide stiffness and strength to the superstructure, are usually aligned along the x-direction and y-direction with reduced interaction between them. Finally, only tangent-stiffness proportional damping is provided to the superstructure to avoid overdamping issues [62][63][64][65], with damping rate equal to 2%, typical value for reinforced concrete structures equipped with seismic isolators [63][64].

3.3 Design of the base isolated system

As already mentioned in Section 2.3, the design of the isolation bearing has been carried out using a set of 100 accelerograms consistent with the target design hazard level, represented by a *MAF* of exceedance ν_d = 0.0021 1/year (probability of exceedance of 10% in 50 years), typical of the

Ultimate Limit State (ULS) according to European standards [4][56]. The aforesaid design hazard level corresponds to the seismic intensity values im_d = 0.173 g for the T_{is}=3.0s isolation system and im_d = 0.071 g for the T_{is} =5.0s. The 100 design accelerograms, generated using the same probabilistic hazard framework previously described, are selected to have *IM*s as close as possible to these target values (im_d). In particular, the total rubber thickness and the diameter of the isolation bearing (h_{is} and D_{is} respectively) as well as the superstructure yielding force (Fy) have been determined by iteratively performing nonlinear time history analysis on each case study with the 100 design accelerograms till attaining an average maximum shear strain value equal to the design one γ_d, and a superstructure average maximum displacement coherent with the overstrength ratio. This procedure, despite cumbersome, has been adopted because of the complex dynamic behaviour of *HDR* bearings, whose equivalent linear properties strongly depends on the shear strain amplitude, as shown in Fig. 6. In fact, despite a more efficient *IM* has been assumed in this work (as described in Section 2.3), design procedures based on simplified linear approaches would lead to a seismic response at the design condition different from the assumed one, due to the record-to record variability of the strongly nonlinear response of *HDR* bearings.

Results of the design are summarized in Table 2, Table 3 and Table 4, where the thickness of the single rubber layer t_r and the compression stress σ are also reported. For completeness, also the normalised yielding force values F_y / Mg (where g is the acceleration of gravity) of the superstructure are reported. As expected, the design features of the isolation systems are the same for the two overstrength ratios Ω/q=1 and Ω/q=2.5, thus confirming that the strength of the superstructure doesn't affect the isolation design.

Regarding the two configuration chosen, the cases with T_{is}=3s can be designed by using both 15 and 8 rubber bearings (Table 2 and Table 3), whereas the cases T_{is}=5s can be designed only by adopting the configuration with 8 rubber bearings and 7 flat sliders (Table 4). A further important remark is about the compression stress (σ) values, which are notably lower than the corresponding critical pressure values at zero displacement σ_{cr} (especially in the cases with T_{is}=3s and 8 bearings), as reported in the tables. Consequently, P-Δ effects due to large displacements are limited, as can be observed in Fig. 6 where numerical cycles are reported for different compression levels, with reference to the bearing with D_{is}= 427mm and h_{is}= 158mm. Only for σ=10 MPa differences are more evident. However, the behaviour at large deformations (for shear strains larger than 3) is always characterized by a significant hardening, that prevent the buckling (zero tangent stiffness) and post-buckling behaviour. As expected, increasing the vertical pressure, G_{eq} decreases in the whole range of shear deformations while ξ_{eq} increases (as can be seen in Fig. 6 b and c respectively). Other bearings with different dimensions (not shown in these figures) are characterized by similar results, due to the limits defined by the codes.

As final remark, it is worth to note that only nominal properties of bearings are considered in designing the isolation systems, neglecting the variability related to the bearings production or ambient conditions. The aim of this work is in fact to focus only on the effect of the considered design parameters on the final reliability of the system, without introducing other source of uncertainties. For the same reason the probabilistic framework illustrated in the previous section account for only the record-to-record variability, whereas other uncertainties (such as the variability of bearing properties or the variability of their shear deformation capacity) are disregarded in this work.

Table 2. Dimensions of the isolation bearings and superstructure yielding force (T_{is} = 3s, 15 *HDR* bearings)

Case	γ_d	D_{is}	h_{is}	t_r	σ	σ_{cr}	F_y/Mg
	[-]	[mm]	[mm]	[mm]	[MPa]	[MPa]	[-]
1	2	393	117	2.8	-5.40	-30.01	0.114
2	1.5	427	158	3.0	-4.56	-23.13	0.111

Case	***γ_d***	***D_{is}***	***h_{is}***	***t_r***	***σ***	***σ_{cr}***	***F_y/Mg***
	[-]	[mm]	[mm]	[mm]	[MPa]	[MPa]	[-]
3	1	476	239	3.4	-3.67	-16.03	0.109
4	2	393	117	2.8	-5.40	-30.01	0.258
5	1.5	427	158	3.0	-4.56	-23.13	0.245
6	1	476	239	3.4	-3.67	-16.03	0.241

Table 3. Dimensions of the isolation bearings and superstructure yielding force (T_{is} = 3s, 8 *HDR* bearings)

Case	***γ_d***	***D_{is}***	***h_{is}***	***t_r***	***σ***	***σ_{cr}***	***F_y/Mg***
	[-]	[mm]	[mm]	[mm]	[MPa]	[MPa]	[-]
7	2	543	119	3.9	-1.99	-44.78	0.122
8	1.5	590	160	4.2	-1.68	-23.13	0.118
9	1	659	244	4.7	-1.35	-23.06	0.114

Table 4. Dimensions of the isolation bearings and superstructure yielding force (T_{is} = 5s, 8 *HDR* bearings)

Case	***γ_d***	***D_{is}***	***h_{is}***	***t_r***	***σ***	***σ_{cr}***	***F_y/Mg***
	[-]	[mm]	[mm]	[mm]	[MPa]	[MPa]	[-]
10	2	383	166	2.8	-3.98	-19.41	0.064
11	2	383	166	2.8	-3.98	-19.41	0.122
12	2	383	166	2.8	-3.98	-19.41	0.258

4 Results: demand hazard curves

This chapter illustrates the results of the parametric probabilistic analysis carried out on the set of 12 case studies previously presented. The response of the various systems is investigated by observing two main parameters: (*i*) the maximum superstructure's relative displacement among the x and y directions, $u_s = \max_t(|u_{sx}(t)|, |u_{sy}(t)|)$; (*ii*) the maximum bearing's shear strain $\gamma_{is} = \max_t \sqrt{u_{bx}(t)^2 + u_{by}(t)^2}\,/h_{is}$.

The outcomes presented in the next subsections are in the form of demand hazard curves. In each figure, two horizontal lines are added: a grey dotted line identifying the design hazard *MAF* ν_d = 0.0021 1/year and a green dashed line representing the target reliability level $\nu_{target} = 2\cdot10^{-4}$ 1/year, consistent with Codes [11][12]. To better understand the influence of the parameters varied within the analysis, two design parameters (e.g., Ω/q and N_{is}) out of three are kept fixed in every chart.

First, the case studies with T_{is}=3s are examined, by discussing the superstructure response (Section 4.1) and the isolation system response (Section 4.2). In Section 4.3, the influence of the isolation period is addressed and results from systems with T_{is}=3s and T_{is}=5s are compared. Finally, in Section 4.4, results are commented from the point of view of the seismic reliability: safer and less safe cases (sets of design parameters) are highlighted, providing a preliminary quantification of the safety factors required to satisfy the target reliability levels.

4.1 Superstructure response

Fig. 7 illustrates the demand hazard curves of the superstructure relative displacement u_s for the cases T_{is}=3s. Charts of Fig. 7 (a, b, and c) compare the curves relating to different values of the design shear strain γ_d (1, 1.5 and 2 respectively), from case 1 to case 9.

In all the figures the initial branches of the curves, representing the elastic range of the superstructure response, are overlapped. This suggests that the elastic behaviour of the superstructure is not affected by the design shear strain γ_d. In other words, the superstructure response is the same despite the isolation stiffness vary in the three cases for shear deformations lower than the design one (due to the different behaviour of the rubber, as depicted in Fig. 6). This can be explained considering two phenomena: first, high T_{is} values usually fall within the range of almost constant displacement spectrum, and second, the high isolation ratio at the design condition (T_{is}/T_s) ensures that almost only the isolation modal component contributes to the superstructure response [1]. The result is a superstructure response which is proportional to the spectral displacement at the isolation period.

In the case Ω/q=1, (Fig. 7 a and c), the superstructure attains the yielding limit at v_d as expected, because no safety margin is taken on the superstructure capacity (base shear strength) at the design stage; once the superstructure attains the yielding condition, the curves reduce its slope and large increment of displacements are observed in conjunction with small reduction of *MAFs*, leading to a fast increase of the superstructure displacement demand related to the plastic response. This confirms that the ductility demand of isolated structure can be very high if the superstructure exceeds its elastic limit [8]. The same behaviour is recognized in the case Ω/q=2.5, but it is postponed (lower *MAF*) due to the larger yielding strength available on the superstructure.

The after-yielding tails of the curves, unlike the elastic branches, have a higher sensitivity to the design shear deformation: curves with higher γ_d values show higher *MAFs* because the hardening of the rubber is attained earlier. The reason is related to the rubber stiffening behaviour that reduces the isolation period, increasing both the base forces and superstructure displacements (which rise faster being the response no longer governed by the spectrum range of constant displacements). Moreover, once the superstructure yields, the T_s value increases (thus the T_{is}/T_s ratio reduces) and the hypothesis that only the isolation period contributes to the superstructure response falls.

Finally, there are no substantial differences between the case of 15 *HDR* bearings (Fig. 7 a) and the case with 8 *HDR* bearings (Fig. 7 c) because, as also shown in Fig. 6 a, vertical pressures lower than 6MPa (see Table 2 to Table 4) only slightly affect the cyclic response of the bearings (i.e. P-Δ effects are not significant given the design limits).

To better highlight the influence of Ω/q on u_s, the curves of Fig. 7 (a and b) are rearranged in Fig. 7 (d, e and f), comparing the cases with Ω/q = 1 and the cases with Ω/q =2.5, namely cases from 1 to 6 (the other two parameters, γ_d and N_{is}, are kept fixed in each chart). Again, the two curves are overlapped in their first branch until the case Ω/q =1 yields. After this point the deformation demand strongly increase for Ω/q =1 while the curve of Ω/q =2.5 continues with the previous slope. To complete this results discussion, an average inter storey drift of 2% is assumed as the threshold value beyond which the superstructure stability could be strongly compromised, i.e., the collapse performance level according to [66]; this threshold is reported in the charts of Fig. 7 (vertical dotted line) in terms of equivalent relative displacement, 0.16m. It can be noted that only the case Ω/q =2.5 fulfils the reliability target (cases 5 and 6), i.e., the collapse condition is attained with a *MAF* lower than $\nu_{target} = 2\cdot10^{-4}$ 1/year (the case 4 is not in compliance but close to it). This concept will be further discussed in the Subsection 4.4 on safety factors.

4.2 Isolation system response

Regarding the rubber shear deformation γ_{is} of the bearings, the demand hazard curves for T_{is}=3s are reported in Fig. 8 (a, b, and c) comparing results obtained by adopting different design shear strains.

Unlike the curves previously showed (related to the superstructure), the slope of shear deformation curves decreases monotonically with the *MAF*, suggesting a controlled increase of the bearing response due to the rubber stiffening behaviour (see Fig. 6 a), that limits the growth of the shear deformation with increasing seismic actions.

The response values at ν_d are in all the cases very close to the design values γ_d, thus confirming the effectiveness of the design procedure described in section 3.3.

To better highlight the influence of Ω/q on γ_{is}, the curves are rearranged in Fig. 8 (d, e, and f), comparing the cases with Ω/q = 1 and the cases with Ω/q =2.5 (γ_d and N_{is} are kept fixed in each chart). In all the cases, the curves are almost overlapped in the whole range of *MAFs*, with only slight discrepancies observed for shear strain values higher than the design ones: this confirms the negligible influence of Ω/q on the isolation response, as also proven in [8]. This can be explained considering that the isolated structure maintains its initial frequency and the predominant isolation mode response even after the superstructure yielding, i.e., the elongation of the superstructure period is not related to an elongation of the isolated period.

To complete this results discussion, thresholds related to the *HDR* bearing capacity are reported in the charts of Fig. 8 d-f (vertical dotted line). Based on the available technical literature [67] a value of 350% of shear strain has been assume as collapse condition of bearings. It can be noted that only the cases with γ_d =1 fulfils the reliability target with a collapse *MAF* lower than the reliability target, whereas the cases with γ_d =1.5 and γ_d =2 are not in compliance with it (even though the case γ_d =1.5 is very close to it). This concept will be further discussed in the Subsection 4.4 from the point of view of safety factors.

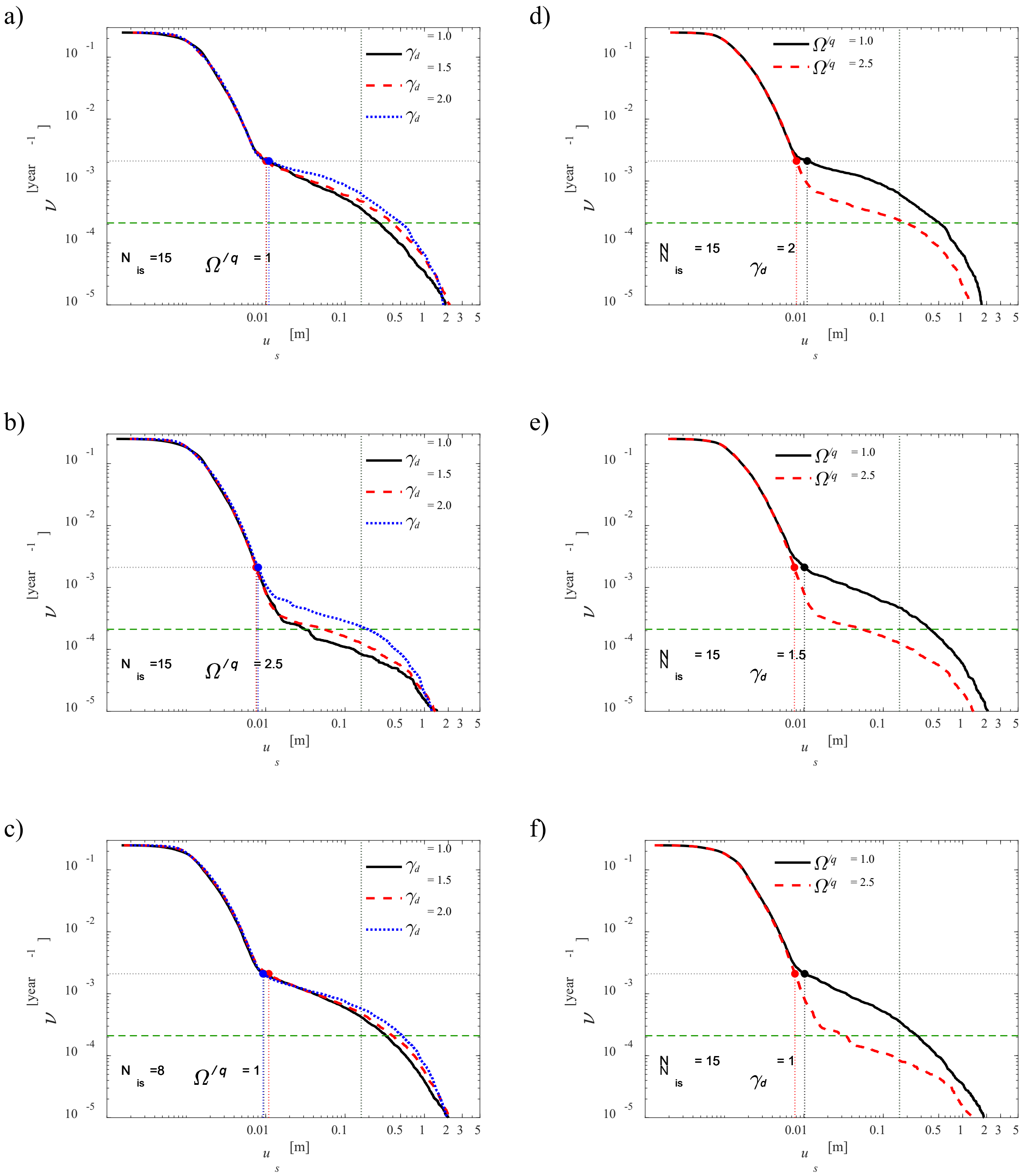

508 Fig. 7. Demand hazard curves of u_s for T_{is}=3s and varying γ_d (a,b,c) or varying Ω/q ratios (d, e, f).

509

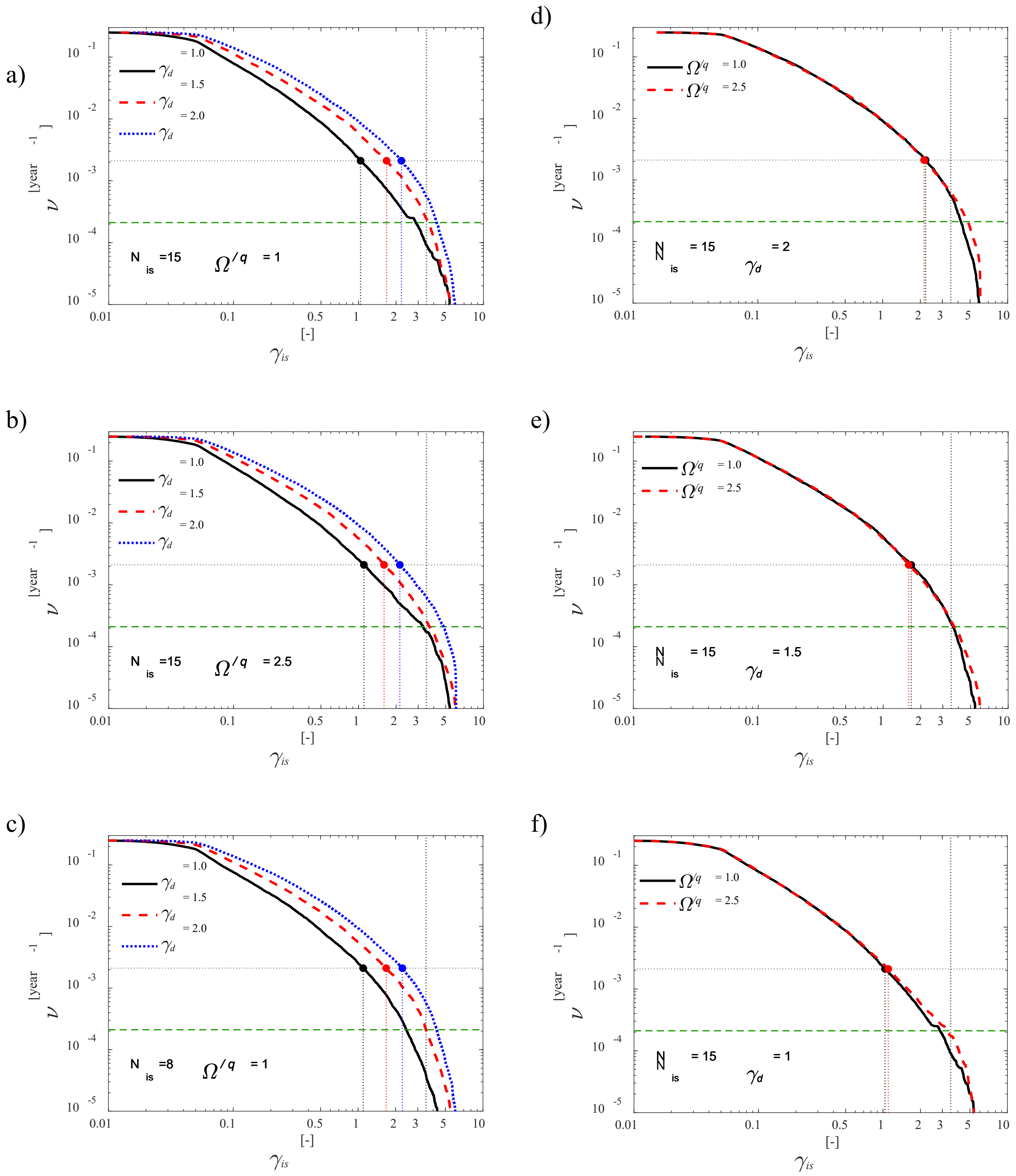

Fig. 8. Demand hazard curves of γ_{is} for T_{is}=3s and varying γ_d (a,b,c) or varying Ω/q ratios (d, e, f).

4.3 Influence of the isolation period

The isolation period is another free parameter which can be defined at the design stage. A direct comparison between the case T_{is}=5s with the previous T_{is} =3s is made in Fig. 9, for the design shear strain γ_d = 2. Regarding the superstructure (Fig. 9 a, c), the first branch of the curves shows a lower displacement demand in the elastic range. This is expected as the cases compared share the same superstructure fixed base period and consequently the same stiffness, but for T_{is}=5s (the red dashed curve) the seismic input filtered by the isolation is lower [1]. On the contrary, after the yielding of the superstructure, the T_{is}=5s curve crosses the case T_{is}=3s, leading to higher displacement demands in the plastic range, confirming that the ductility demand increases with the isolation period [8]. Conversely, the isolation shear deformation demand does not vary sensibly from the case T_{is} =3s to the case T_{is} =5s (Fig. 9 b, d).

However, it should be noted that the comparison presented here between T_{is}=3s and T_{is} =5s, although coherent in terms of design procedure, is made on two superstructures with strong differences in terms of actual strength; indeed, the superstructures corresponding to T_{is} =5s (cases 10 and 11) are characterised by a normalised yielding force (see F_y/Mg in Table 2 and Table 4) almost half the values of the corresponding cases (4 and 5) with T_{is} =3s. Consequently, the superstructure design for isolation systems with T_{is} =5s is mostly expected to be governed by minimum code requirements or non-seismic actions (gravity and wind loads); moreover, in these cases, the contribution provided by non-structural elements to the actual strength of the system is relatively higher than the cases with T_{is} =3s. The case study 12 (T_{is}=5s and Ω/q=4.75, blue dotted line) shown in Fig. 9 c and characterised by the same superstructure of case 4 (the higher Ω/q ratio stems from the lower design seismic demand), is added to represent this specific condition. This last case shows a significant reduction of u_s with respect to both the case 11 (T_{is}=5s and Ω/q=2.5 red dashed line) and the case 4 (T_{is}=3s and Ω/q=2.5 black solid line), hence confirming that, with the same superstructure, an enhancement of the structural performance can be achieved increasing the isolation period. Moreover, since the superstructures are the same but the total volume of *HDR* bearings in case 12 is lower than case 4, also a cost reduction could be pursued by increasing the isolation period T_{is}.

Regarding γ_{is} (Fig. 9 d), no variations are observed, confirming that nor the isolation period neither the overstrength ratio affect the isolation response.

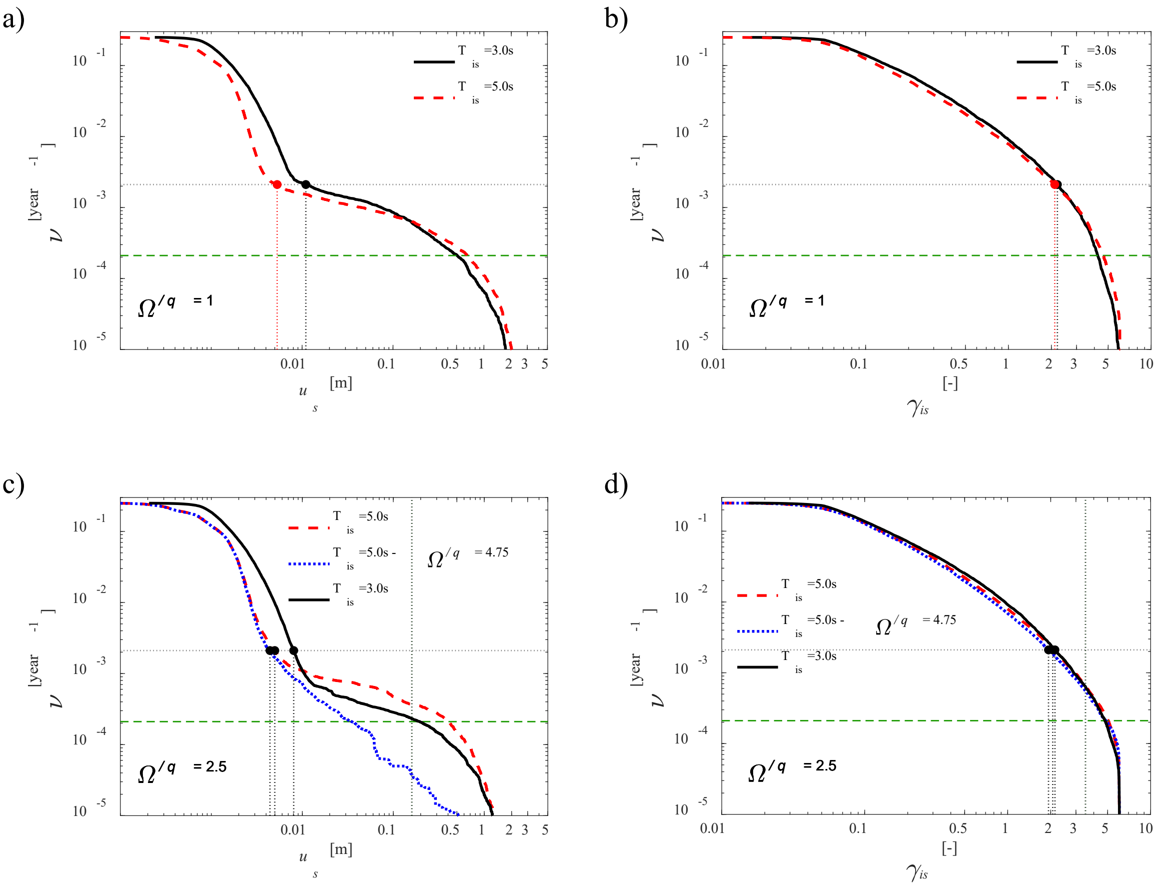

Fig. 9. Demand hazard curves of u_s (a, c) and γ_{is} (b, d) for T_{is}=5 s and T_{is}=3 s. γ_d=2.

4.4 Safety Factors

Table 5 summarises the main results obtained from the probabilistic analysis. Indeed, the following information are collected for each response parameter (u_s and γ_{is}) and for every case study examined (from case 1 to case 12): case study number; principal design parameters; target design response values u_d and γ_d; achieved response values at the reference design *MAF* level ν_d ($u_s(\nu_d)$ and $\gamma_{is}(\nu_d)$) and at the target reliability level ν_{target} (u_s (ν_{target}) and $\gamma_{is}(\nu_{target})$); estimates of the required reliability factors $\boldsymbol{R_\gamma}$ (explained hereafter) for the isolation shear strain.

The $\boldsymbol{R_\gamma}$-factor is defined as the ratio between the response parameter γ_{is} evaluated at a given *MAF* level, ν, and the corresponding design value γ_d:

$$\boldsymbol{R}_{\gamma}(\nu, \gamma_{is}) = \frac{\gamma_{is}(\nu)}{\gamma_d} \quad (5)$$

It is worth to note that the $\boldsymbol{R}_{\gamma}$-factor can be interpreted as reliability factor, which applied to the design value of the parameter provides a demand value consistent to the specified target *MAF* (ν_{target}= 2.1·10^{-4} 1/year in this study). On the other hand, $\boldsymbol{R}_{\gamma}$ can be used as reliability factor to define the minimum isolator's shear capacity to be tested (given both ν_d and a ν_{target}).

Examining the values of Table 5 some important comments can be made. For what concerns the isolation system, it is possible to observe how the response values estimated at the reference *MAF* ν_d (2.1·10^{-3} 1/year), $\gamma_{is}(\nu_d)$, are very close to the target design ones γ_d (1, 1.5 and 2), due to the advanced design procedure adopted. Furthermore, by looking at the shear strain values $\gamma_{is}(\nu_{target})$, one can observe that the demand values are significantly larger than the minimum shear strain capacity values required by the European code on anti-seismic devices [4]. In fact, the code prescription for rubber bearings is to carry out a ramp test up to a displacement equal to the design displacement γ_d amplified by two factors: a magnification factor of 1.2 aimed at increasing the reliability of the structural system and a further partial factor of 1.15. Applied to the current cases (i.e., γ_d = 1, 1.5, 2), the Code requirements would lead to values of maximum shear deformation capacity equal to 1.38, 2.07 and 2.76 respectively, which are all significantly lower than the related demand values $\gamma_{is}(\nu_{target})$ in Table 5. This result suggests that larger amplification factors should be applied to γ_d to attain reliability levels consistent with the Codes requirements. Moreover, $\boldsymbol{R}_{\gamma}$ factors decrease as the design shear strain increases due to the more pronounced hardening behaviour of the isolation bearings, leading to the conclusion that different reliability factors should be tailored for different behaviours of the isolation devices. A similar result was achieved in another recent work [3], where, however, a different design *MAF* (ν_d) was used (coherent with American standards [5] prescriptions), thus a direct comparison between values stemming from the present work and the one in [3] cannot be made.

Table 5. Seismic demand values attained at design ($\nu_d = 2.1 \cdot 10^{-3}$ 1/year) and target ($\nu_{target} = 2.1 \cdot 10^{-4}$ 1/year) *MAF* levels, and reliability factor $\boldsymbol{R_\gamma}$

Case	***Design features***	γ_d [-]	u_d [mm]	$\gamma_{is}(\nu_d)$ [-]	$\gamma_{is}(\nu_{target})$ [-]	R_γ [-]	$u_s(\nu_d)$ [mm]	$u_s(\nu_{target})$ [mm]
1	T_{is} = 3.0s N_{is}=15 Ω/q =1.0	2	7.1	2.20	4.26	**2.13**	10.99	529.10
2		1.5	6.9	1.68	3.67	**2.45**	10.14	409.12
3		1	6.8	1.04	2.92	**2.92**	10.21	282.86
4	T_{is} = 3.0s N_{is}=15 Ω/q =2.5	2	6.4	2.14	4.85	**2.42**	8.05	209.95
5		1.5	6.1	1.60	3.77	**2.51**	7.58	60.68
6		1	6.0	1.10	3.32	**3.32**	7.70	35.06
7	T_{is} = 3.0s N_{is} =8 Ω/q =1.0	2	7.6	2.26	4.28	**2.14**	9.26	542.63
8		1.5	7.3	1.68	3.53	**2.35**	10.93	416.05
9		1	7.1	1.10	2.47	**2.47**	9.45	340.81
10	T_{is} = 5.0s N_{is} =8 Ω/q =1.0	2	4.0	2.11	4.67	**2.34**	5.31	676.70
11	T_{is} = 5.0s N_{is} =8 Ω/q =2.5	2	3.2	2.06	5.10	**2.55**	4.98	416.37
12	T_{is} = 5.0s N_{is} =8 Ω/q =4.75	2	3.2	1.93	4.98	**2.49**	4.41	37.87

For what concerns the superstructure, most of the comments made for the isolation response still apply. The response values at ν_{target}, $u_s(\nu_{target})$, are always higher than the threshold values of 160mm previously introduced (i.e., corresponding to 2% inter-storey drift and denoting the collapse conditions according to [66]), except for three cases out of 12 (namely cases 5, 6 and 12), confirming that the current seismic code prescriptions may not ensure the achievement of the reliability target. As expected, the case 12 (same superstructure strength of case 4 but isolation at T_{is} = 5.0s) has the best performance in terms of u_s.

Finally, it is important to remember that the systems' probabilistic response (thus the seismic risk) associated to the design procedures is hazard- (and thus site-) dependent [21][23]. Consequently, the results presented in this paper (concerning both the isolation system and the superstructure) could vary in absolute terms by changing the hazard, although the observed trends would remain of general validity.

5 Conclusions

In this study the seismic reliability of structural systems isolated with *HDR* bearings has been investigated, using a robust probabilistic framework combined with advanced numerical models for the isolation system, accounting for both the hardening and the P-Δ effect. A parametric study has been carried out by varying the design parameters of both the isolation system and the superstructure to assess their influence on the final seismic reliability of the isolated structure. For each variated design condition, the demand hazard curves of the monitored response parameters, related to both superstructure (relative displacement u_s) and isolation system (rubber shear strain γ_{is}), have been computed. The following conclusions can be drawn from the obtained results.

- Among the design parameters investigated, design shear strain of the rubber bearings (γ_d), superstructure overstrength ratio (Ω/q) and isolation period (T_{is}) strongly influence the final reliability of the system in terms of superstructure relative displacement u_s, also showing a strong interdependency, especially between Ω/q and T_{is}. The design shear strain γ_d is the only relevant parameter influencing the response of the isolation system (i.e., affecting the γ_{is} hazard curve). The effects of the percentage of flat sliders (i.e., bearing shape factors) is instead negligible on both u_s and γ_{is} as the P-Δ effect is not significant.

- For what concerns the superstructure response, increments of the overstrength ratio Ω/q notably affect the post-elastic branches of the u_s hazard curves, where a strong reduction of the *MAF* of exceedance can be observed. A value Ω/q = 2.5 is needed for the case T_{is} = 3.0s to achieve a *MAF* at the collapse threshold (average inter storey drift of 2%) lower than the target reliability. Moreover, a further slight reduction of the superstructure failure probability is observed for lower design shear strains γ_d due to the smaller stiffening behaviour of the rubber during the plastic stage of the superstructure. The value of Ω/q should be further increased (beyond 2.5) in the case of T_{is} = 5.0s to have a *MAF* lower than the target reliability level.
- Regarding the isolation system, the seismic demand γ_{is} increases with the design shear strain γ_d. If a bearing shear deformation capacity of 350% is assumed, only the cases with γ_d = 1 show a *MAF* of collapse lower than the reliability target. All the other design parameters have a negligible influence on the isolation response.
- Increasing the isolation period up to T_{is} = 5.0s, and keeping fixed all the other design parameters, both the isolation bearing diameter and the superstructure strength reduces significantly, while the total rubber thickness slightly increases. The u_s hazard curve of T_{is} = 5.0s shows a lower displacement demand in the elastic range with respect to the case T_{is} = 3.0s; conversely, once yielded, the T_{is}=5s hazard curve crosses the T_{is}=3s one, leading to a higher displacement demand in the plastic range, which confirms that the ductility demand increases with the isolation period for a given Ω/q value.
- The case T_{is} = 5.0s and Ω/q =4.75 represents the most reliable solution in terms of u_s. It is worth to note that this solution is not expensive as might appear, being the superstructure the same

considered in the case T_{is} = 3.0s and Ω/q =2.5. Considering this result, the isolation period represents a design parameter that should be maximised to obtain the twofold aim of higher structural performance and total cost reduction.

- The European code on seismic devices (EN 15129) prescribes to carry out a shear capacity test at a shear strain equal to 1.2·1.15 times the design value γ_d; according to the outcomes of the present analysis, the shear strain values stemming from the application of such Code requirement do not allow achieving satisfactory reliability levels (i.e., the corresponding *MAFs* are much higher than the reliability target).
- Values of the reliability factors for γ_d are provided, which can be also interpreted as amplification coefficients of the design values to achieve the required reliability level and thus to define the minimum shear capacity to be tested;
- The obtained reliability factors depend on the specific design values chosen for the *HDR* bearing shear strain, showing that the current single reliability factor does not ensure a satisfactory reliability level and that this approach is not actually easy to use in the current codes;

It is important to remember that all these results are strongly related to the hazard selected for the analyses, thus wider seismic reliability assessment procedures considering different sites should be adopted and/or risk-based design approaches should be investigated. Moreover, for a revision/improvement of the current Codes the results should also be confirmed by considering more complex structural systems (also explicitly including the presence of non-structural components).

Finally, other sources of uncertainties (such those related to the superstructure and bearings properties variation within tolerance limits imposed by the codes) should be accounted for both in the design procedure and in the probabilistic framework in order to assess the effectiveness of the approaches suggested by the codes (i.e. upper/lower bound analysis). The uncertainty about the shear capacity of bearings could be also introduced, if sufficient experimental data are available.

References

[1] Kelly JM. (1997) *Earthquake-resistant Design with Rubber* (2^{nd} edition). Springer: London, 1997

[2] Christopoulos, C., Filiatrault, A. (2006). *Principles of Passive Supplemental Damping and Seismic Isolation* - IUSS Press - Eucentre Press. Pavia, Italy

[3] Zayas V, Mahin S and Constantinou MC (2017) *Seismic Isolation Standard For Continued Functionality*. Technical Report: UCB/SEMM-2017/03

[4] CEN [2009] EN15129. Antiseismic Devices, Brussels, Belgium.

[5] ASCE 7 (2016) "*Minimum Design Loads and Associated Criteria for Buildings and Other Structures*", American Society Of Civil Engineers

[6] Kitayama S, Constantinou MC. *Collapse performance of seismically isolated buildings designed by the procedures of ASCE/SEI 7*. Engineering Structures 2018; 164: 243–258. DOI: 10.1016/j.engstruct.2018.03.008.

[7] Shao B, Mahin SA, Zayas V. *Achieving targeted levels of reliability for low-rise seismically isolated structures*. Soil Dynamics and Earthquake Engineering 2019; 125: 105744. DOI: 10.1016/j.soildyn.2019.105744.

[8] Kikuchi, M., Black, C.J., Aiken, I.D., (2008). *On the response of yielding seismically isolated structures*. Earthquake Engng Struct. Dyn. 37, 659–679. https://doi.org/10.1002/eqe.777

[9] Cardone D, Flora A, Gesualdi G. (2013) *Inelastic response of RC frame buildings with seismic isolation*. Earthquake Engineering & Structural Dynamics; 42(6): 871–889. DOI: 10.1002/eqe.2250.

[10] Tsiavos A, Mackie KR, Vassiliou MF, Stojadinović B. *Dynamics of inelastic base-isolated structures subjected to recorded ground motions*. Bulletin of Earthquake Engineering 2017; 15(4): 1807–1830. DOI: 10.1007/s10518-016-0022-5.

[11] Fajfar, P. (2018). *Analysis in seismic provisions for buildings: past, present and future*. The fifth Prof. Nicholas Ambraseys lecture. Bull Earthquake Eng 16, 2567–2608

[12] Gkimprixis A, Tubaldi E, Douglas J (2019*) Comparison of methods to develop risk targeted seismic design maps*. Bull Earthq Eng 2019;17(7):3727–52.

[13] Dall'Asta A, Scozzese F, Ragni L, Tubaldi E. (2017) *Effect of the damper property variability on the seismic reliability of linear systems equipped with viscous dampers*. Bull Earthq Eng, 15:5025–53. doi:10.1007/s10518-017-0169-8

[14] Scozzese F., Tubaldi E., Dall'Asta A. (2019). *Seismic risk sensitivity of structures equipped with anti-seismic devices with uncertain properties*. Structural Safety, Vol.77, 30-47

[15] Dall'Asta A, Tubaldi E, Ragni L. (2016). *Influence of the nonlinear behavior of viscous dampers on the seismic demand hazard of building frames*. Earthq Eng Struct Dyn;45:149–69. doi:10.1002/eqe.2623

[16] Scozzese, F., Gioiella, L., Dall'Asta, A., Ragni, L., Tubaldi, E., 2021. *Influence of viscous dampers ultimate capacity on the seismic reliability of building structures*. Structural Safety 91, 102096. https://doi.org/10.1016/j.strusafe.2021.102096.

[17] Miyamoto HK, Gilani ASJ, Wada A, and Ariyaratana C (2011). *Identifying the Collapse Hazard of Steel Special Moment-Frame Buildings with Viscous Dampers Using the FEMA P695 Methodology*, Earthquake Spectra, Volume 27, No. 4, pages 1147–1168

[18] Kitayama, S and Constantinou MC (2019). *Probabilistic seismic performance assessment of seismically isolated buildings designed by the procedures of ASCE/SEI 7 and other enhanced criteria*. Engineering Structures 179, 566–582.

[19] Nakazawa T., Kishiki S., Qu Z., Miyoshi A., Wada A. (2011). *Fundamental Study on Probabilistic Evaluation of the Ultimate State of Base Isolated Structures*, Proceedings, 8th International Conference on Urban Earthquake Engineering, Tokyo Institute of Technology, Tokyo, Japan

[20] Ragni L, Micozzi F, Tubaldi E, Dall'Asta A. (2020) Behaviour of Structures Isolated by HDNR Bearings at Design and Service Conditions. Journal of Earthquake Engineering, DOI: 10.1080/13632469.2020.1776792

[21] Iervolino I, Spillatura A, Bazzurro P. (2018). Seismic Reliability of Code-Conforming Italian Buildings. Journal of Earthquake Engineering; 22, 5-27.

[22] Ragni L, Cardone D, Conte N, Dall'Asta A, Di Cesare A, Flora A, Leccese G, Micozzi F, Ponzo C. (2018) Modelling and seismic response analysis of Italian code-conforming base-isolated buildings. Journal of Earthquake Engineering; 22, 198-230.

[23] F. Micozzi, A. Flora, L.R.S. Viggiani, D. Cardone, L. Ragni & A. Dall'Asta (2021): *Risk Assessment of Reinforced Concrete Buildings with Rubber Isolation Systems Designed by the Italian Seismic Code*, Journal of Earthquake Engineering, DOI: 10.1080/13632469.2021.1961937

[24] Ponzo FC, Di Cesare A, Telesca A, Pavese A, Furinghetti M. *Advanced Modelling and Risk Analysis of RC Buildings with Sliding Isolation Systems Designed by the Italian Seismic Code*. Applied Sciences 2021; 11(4): 1938. DOI: 10.3390/app11041938.

[25] Furinghetti, M., Pavese, A., Quaglini, V., & Dubini, P. (2019). Experimental investigation of the cyclic response of double curved surface sliders subjected to radial and bidirectional sliding motions. *Soil Dynamics and Earthquake Engineering*, 117, 190-202.

[26] S.K. Au, J.L. Beck, Estimation of small failure probabilities in high dimensions by subset simulation, Probabilistic Engineering Mechanics. 16 (2001) 263–277. doi:10.1016/S0266-8920(01)00019-4.

[27] S.K. Au, Y. Wang, Engineering Risk Assessment with Subset Simulation, 2014. doi:10.1002/9781118398050.

[28] Perotti F, Domaneschi M, De Grandis S. The numerical computation of seismic fragility of base-isolated Nuclear Power Plants buildings. Nuclear Engineering and Design 2013; 262: 189–200. DOI: 10.1016/j.nucengdes.2013.04.029.

[29] Forni M, Poggianti A, Bianchi F, Forasassi G, Lo Frano R, Pugliese G, et al. Seismic Isolation of the IRIS Nuclear Plant. Volume 8: Seismic Engineering, ASME 2009 Pressure Vessels and Piping Conference. Prague, Czech Republic: ASMEDC; 2009. DOI: 10.1115/PVP2009-78042.

[30] Nishida A, Choi B, Yamano H, Takada T. Development of Seismic Countermeasures Against Cliff Edges for Enhancement of Comprehensive Safety of Nuclear Power Plants: Cliff Edges Relevant to NPP Building System. Volume 8: Seismic Engineering, ASME 2018 Pressure Vessels and Piping Conference. Prague, Czech Republic: ASME; 2018. DOI: 10.1115/PVP2018-85066.

[31] Kikuchi M, Nakamura T, Aiken ID. (2010) Three-dimensional analysis for square seismic isolation bearings under large shear deformations and high axial loads. Earthquake engineering and structural dynamics; 39:1513–1531.

[32] Ishii K and Kikuchi M (2018) Improved numerical analysis for ultimate behavior of elastomeric seismic isolation bearings. Earthquake engineering and structural dynamics, 48(1), 65-77.

[33] Kikuchi M and Aiken ID (1997) An Analytical Hysteresis Model for Elastomeric Seismic Isolation Bearings, Earthquake Engineering and Structural Dynamics, 26(2):215-231.

[34] Rubinstein RY, Kroese DP (2017) Simulation and the Monte Carlo Method

[35] Jayaram N, Baker JW (2010) Efficient sampling and data reduction techniques for probabilistic seismic lifeline risk assessment. Earthquake Engineering and Structural Dynamics 39:1109–1131

[36] Cornell CA, Jalayer F, Hamburger RO, Foutch DA (2002) Probabilistic Basis for 2000 SAC Federal Emergency Management Agency Steel Moment Frame Guidelines. Journal of Structural Engineering 128:526–533. doi: 10.1061/(ASCE)0733-9445(2002)128:4(526)

[37] Cornell, C.A.; Krawinkler, H. Progress and challenges in seismic performance assessment. Peer Cent. News 2000, 4, 1–3.

[38] , R.D.; Bertero, V.V. Performance-based seismic engineering: The need for a reliable conceptual comprehensive approach. Earthq. Eng. Struct. Dyn. 2002, 31, 627–652

[39] Aslani, H.; Miranda, E. Probability-based seismic response analysis. Eng. Struct. 2005, 27, 1151–1163

[40] F. Jalayer, J.L. Beck, Effects of two alternative representations of ground-motion uncertainty on probabilistic seismic demand assessment of structures, Earthquake Engineering and Structural Dynamics. 37 (2008) 61–79. doi:10.1002/eqe.745.

[41] D.M. Boore, Simulation of Ground Motion Using the Stochastic Method, in: Seismic Motion, Lithospheric Structures, Earthquake and Volcanic Sources: The Keiiti Aki Volume, Birkhäuser Basel, Basel, 2003: pp. 635–676. doi:10.1007/978-3-0348-8010-7_10.

[42] G.M. Atkinson, W. Silva, Stochastic modeling of California ground motions, Bulletin of the Seismological Society of America. 90 (2000) 255–274. doi:10.1785/0119990064.

[43] S.K. Au, J.L. Beck, Subset Simulation and its Application to Seismic Risk Based on Dynamic Analysis, Journal of Engineering Mechanics. 129 (2003) 901–917. doi:10.1061/(ASCE)0733-9399(2003)129:8(901).

[44] S.L. Kramer, Geotechnical Earthquake Engineering, Prentice-Hall: Englewood Cliffs, NJ., 2003.

[45] Hong, H. P., & Liu, T. J. (2014). Assessment of coherency for bidirectional horizontal ground motions and its application for simulating records at multiple stations. Bulletin of the Seismological Society of America, 104(5), 2491-2502.

[46] Baker, J. W., & Cornell, C. A. (2006). Correlation of response spectral values for multicomponent ground motions. Bulletin of the seismological Society of America, 96(1), 215-227.

[47] Taflanidis, A. A., & Beck, J. L. (2009). Life-cycle cost optimal design of passive dissipative devices. *Structural Safety*, *31*(6), 508-522.

[48] Altieri, D., Tubaldi, E., De Angelis, M., Patelli, E., & Dall'Asta, A. (2018). Reliability-based optimal design of nonlinear viscous dampers for the seismic protection of structural systems. *Bulletin of Earthquake Engineering*, *16*(2), 963-982.

[49] D.M. Boore, W.B. Joyner, *Site amplifications for generic rock sites*, Bulletin of the Seismological Society of America. 87 (1997) 327–341. http://www.bssaonline.org/content/87/2/327.short (accessed 22 January 2018).

[50] Grant Damian N. Response Spectral Matching of Two Horizontal Ground-Motion Components. Journal of Structural Engineering 2011; 137(3): 289–297. DOI: 10.1061/(ASCE)ST.1943-541X.0000227.

[51] Boore DM. *Orientation-Independent, Nongeometric-Mean Measures of Seismic Intensity from Two Horizontal Components of Motion*. Short Note. Bulletin of the Seismological Society of America 2010; 100(4): 1830–1835. DOI: 10.1785/0120090400.

[52] Kohrangi, M., Kotha, S. R., & Bazzurro, P. (2018). Ground-motion models for average spectral acceleration in a period range: direct and indirect methods. Bulletin of Earthquake Engineering, 16(1), 45-65.

[53] Chioccarelli, E., Cito, P., Iervolino, I., & Giorgio, M. (2019). REASSESS V2. 0: software for single-and multi-site probabilistic seismic hazard analysis. Bulletin of Earthquake Engineering, 17(4), 1769-1793.

[54] Mullins, L. 1969. Softening of rubber by deformation. Rubber Chemistry and Technology 42 (1): 339–62. doi: 10.5254/1.3539210.

[55] Scozzese, F., Tubaldi, E., & Dall'Asta, A. (2020). Assessment of the effectiveness of Multiple-Stripe Analysis by using a stochastic earthquake input model. Bulletin of Earthquake Engineering, 1-37.

[56] CEN. EN 1998-1. Eurocode 8: Design of structures for earthquake resistance - Part 1: General rules, seismic actions and rules for buildings, Brussels, Belgium, 2005.

[57] Mitchell, D., Paultre, P., (1994). Ductility and overstrength in seismic design of reinforced concrete structures. Can. J. Civ. Eng. 21, 1049–1060. https://doi.org/10.1139/l94-109

[58] Koh, C. G., and Kelly, J. M. (1986). ''Effects of axial load on elastomeric bearings.'' UCB/EERC-86/12, Earthquake Engrg. Res. Ctr., University of California, Berkeley, Calif.

[59] McKenna, F., (2011). OpenSees: A Framework for Earthquake Engineering Simulation. Computing in Science Engineering 13, 58–66.

[60] Bridgestone Corporation (2017) Seismic isolation product line-up.

[61] Takaoka E, Takenaka Y, Nimura A. Shaking table test and analysis method on ultimate behavior of slender base-isolated structure supported by laminated rubber bearings. Earthquake Engineering & Structural Dynamics 2011; 40(5): 551–570. DOI: 10.1002/eqe.1048.

[62] Ryan KL, Polanco J. Problems with Rayleigh Damping in Base-Isolated Buildings. Journal of Structural Engineering 2008; 134(11): 1780–1784. DOI: 10.1061/(ASCE)0733-9445(2008)134:11(1780).

[63] Pant DR, Wijeyewickrema AC, ElGawady MA. Appropriate viscous damping for nonlinear time-history analysis of base-isolated reinforced concrete buildings. Earthquake Engineering & Structural Dynamics 2013; 42(15): 2321–2339. DOI: 10.1002/eqe.2328.

[64] Anajafi H, Medina RA, Santini‐Bell E. Effects of the improper modeling of viscous damping on the first-mode and higher-mode dominated responses of base-isolated buildings. Earthquake Engineering & Structural Dynamics 2020; 49(1): 51‐73. DOI: 10.1002/eqe.3223.

[65] Hall JF. Discussion of 'Modelling viscous damping in nonlinear response history analysis of buildings for earthquake excitation' by Anil K. Chopra and Frank McKenna: Discussion of A. Chopra and F. McKenna. Earthquake Engineering & Structural Dynamics 2016; 45(13): 2229–2233. DOI: 10.1002/eqe.2761.

[66] FEMA. Hazus Earthquake Model Technical Manual. 2020

[67] Nishi T, Suzuki S, Aoki M, Sawada T, Fukuda S. International investigation of shear displacement capacity of various elastomeric seismic-protection isolators for buildings. Journal of Rubber Research 2019; 22(1): 33–41. DOI: 10.1007/s42464-019-00006-x.